# Simulation of the bulk and surface modes supported by a diamond lattice of metal wires

M. A. Shapiro,[1,a)] K. R. Samokhvalova,[1] J. R. Sirigiri,[1] R. J. Temkin,[1] and G. Shvets[2]
[1]*Plasma Science and Fusion Center, Massachusetts Institute of Technology, Cambridge, Massachusetts 02139, USA*
[2]*Department of Physics, University of Texas at Austin, Austin, Texas 78712, USA*

(Received 3 April 2008; accepted 4 October 2008; published online 18 November 2008)

We present a numerical study of the electromagnetic properties of the three-dimensional metallic wire lattices operating at microwave frequencies with applications to advanced accelerating structures and microwave sources. The metallic lattices can be considered as "artificial plasmas" because they demonstrate the properties of plasmas with a negative dielectric constant. Bulk modes in a diamond lattice of metal wires and surface modes on its interface are calculated. It is shown that the lattice can be modeled as an anisotropic medium with spatial dispersion. In contrast to a simple cubic lattice, the diamond lattice allows the existence of three different interfaces—one isotropic and two anisotropic. The surface modes supported by these interfaces are affected by spatial dispersion, in sharp contrast with the surface mode on an isotropic vacuum/plasma interface. For particle accelerator applications, we identify the electromagnetic mode confined by a plasmonic waveguide formed as a defect in a diamond lattice. All deleterious higher order modes excited as wakefields from the accelerating particle are found to be leaky. The diamond lattice is also useful as a research tool for studying particle radiation in media with spatial dispersion. © *2008 American Institute of Physics*. [DOI: 10.1063/1.3021310]

## I. INTRODUCTION

This paper presents theoretical studies of a three-dimensional (3D) metallic lattice structure useful for accelerator and vacuum electron device applications. The lattice is built of metallic wires of square or round cross section. The wires intersect in the nodes of a diamond lattice [Fig. 1(a)]. The wires themselves act as the bonds in the diamond lattice. A diamond lattice made of metallic wires has been previously proposed in Ref. 1 and theoretically and experimentally studied in the microwave range. In this paper, we calculate the bulk modes and the surface modes on the interface of the diamond wire lattice and propose an accelerator structure operating in a defect mode in the diamond lattice.

The 3D metallic lattice is an "artificial plasma" with a negative dielectric constant.[1–3] The lattice supports a surface mode at the interface of the lattice and vacuum. The surface mode decays in both directions, namely, vacuum and lattice. Such an effect is possible only if the dielectric constant is negative. The surface mode on the interface of the lattice can be employed in a surface mode accelerator.[4] A surface mode accelerator is of interest for operation at higher microwave frequencies (up to 90 GHz) and also for laser acceleration at infrared wavelengths. The wire lattice is a medium with spatial dispersion (SD).[5–7] The effect of SD on the transition radiation of charged particles has been theoretically studied.[8] It is shown that the radiation into longitudinal surface waves is specific for the medium with SD. Radiation of a charged particle moving above the interface of a medium with SD (Smith–Purcell radiation) or impinging on to the interface (transition radiation) can be modeled for the diamond lattice.

3D metallic lattices are photonic (electromagnetic) crystals which have the potential for interesting applications as accelerator structures and microwave tube circuits. We have conducted experiments on a 17 GHz photonic band gap (PBG) accelerator structure.[9] The PBG accelerator structure was built as a disk-loaded waveguide of six cells. Each cell of this structure was designed as a two-dimensional (2D) array of metal rods with a defect in the center. The defect mode serves as a $TM_{01}$-like accelerating mode. Higher order modes (HOMs), excited as wakefields radiated by a high power electron beam, can result in beam breakup. Such modes are suppressed in a PBG structure. Cold test of the PBG structure showed[10] that the HOMs are suppressed, providing hope that beam breakup can be avoided with these structures. A similar structure is one made of metallic wire structures ("jungle gym" structures), which have been previously utilized as accelerator structures.[11,12] These periodic waveguide structures contained a few wires per period which were set transverse to the waveguide axis. The metallic wire lattice structures discussed in this paper are similar, but they contain extended wire structures. Complex 3D metallic structures may provide more possibilities for wakefield suppression. This paper reports on the basic properties of 3D metallic lattices for possible applications in accelerators and microwave sources. The lattice properties such as the band gaps can be used for designing the accelerator structure. By choosing appropriate lattice parameters, the band gap can be designed such that the accelerating mode is in the band gap and therefore is confined whereas the HOMs, responsible for deflecting the electron beam, are in the propagation band and leak out of the structure. We have also conducted experiments on Smith–Purcell radiation and transition radiation

[a)]Electronic mail: shapiro@psfc.mit.edu.

 

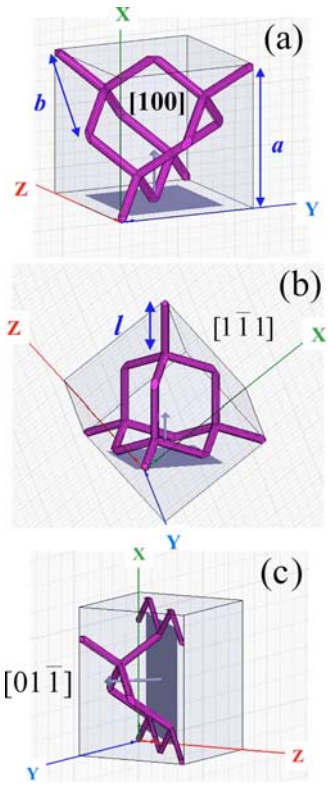


FIG. 1. (Color online) Cubic cell of diamond wire lattice [(a) and (b)]. (a) Anisotropic interface (100) is determined by the crystallographic direction [100]. The surface wave can propagate in the $[01\bar{1}]$ direction. (b) Isotropic interface (111) is determined by the $[1\bar{1}1]$ direction. The surface wave can propagate in the directions [111] and $[11\bar{1}]$. (c) Anisotropic interface (011) is determined by the $[01\bar{1}]$ direction. The surface wave can propagate in the [100] direction.

from electron bunches for use as a bunch length diagnostic.[13–15] The radiation from the electron bunches can be enhanced if the bunch traverses a medium with negative dielectric constant or moves above the medium surface.[4,8] Basic research on a 3D metallic wire medium is thus potentially useful for beam diagnostics applications.

The disk-loaded PBG accelerator structure[9] utilizes a 2D array of metallic rods placed between the disks. The wakefields bounce between the disks and leak out through the array. In this paper, we propose a new approach for an accelerator structure based on a 3D metallic wire lattice. The 3D metallic lattice allows us to build an accelerator structure without any disks. In such a structure, wakefields as HOMs would naturally leak out of the structure without being trapped between the disks. Photonic crystals and photonic crystal fibers have been proposed for laser based acceleration.[16,17] Laser accelerators may benefit from the present study of advanced 3D metallic structures intended for microwave frequencies. In fact, the technology of fabricating diamond lattices for optics has been developed (see Ref. 18 and references therein) and can be used for laser accelerator structures.

The paper is organized as follows. In Sec. II, we simulate the bulk modes in a diamond wire lattice. In Sec. III, we derive the tensor of the effective dielectric constant for a diamond wire lattice. In Sec. IV, we calculate the surface

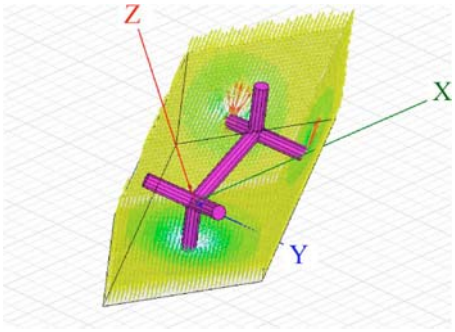


FIG. 2. (Color online) Simulation of bulk modes in the diamond wire lattice using the primitive cell. A longitudinal plasma mode at 6.25 GHz is shown for the lattice cubic cell length $a=2.3$ cm and the wire radius $r=0.07$ cm.

modes. In Sec. V, we discuss the effect of SD on surface modes. In Sec. VI, we propose a plasmonic waveguide formed as a defect in a diamond wire lattice. Sections VII and VIII contain discussion and conclusions, respectively.

## II. BULK MODES

A cubic cell of the diamond wire lattice is presented in Figs. 1(a) and 1(b). We present the simulation results from the diamond lattice carried out using the high frequency structure simulator (HFSS) code.[19] The diamond wire lattice shown in the example was analyzed for the following parameters: cubic unit cell length $a=2.3$ cm, wire section length $l=a\sqrt{3}/4=1$ cm, period of the lattice on the interface $b=a/\sqrt{2}=1.63$ cm, and wire radius $r=0.07$ cm; these are the same parameters as in Ref. 1.

The cutoff (plasma) frequency $f_p=6.25$ GHz was calculated using the primitive cell of the lattice, a rhombohedron shown in Fig. 2. This result agrees with the simulations in Ref. 1 carried out using a different method. The zero-phase advance boundary conditions were applied on the sides of the primitive cell to calculate the plasma frequency. The plasma wave at a frequency of 6.25 GHz is depicted in Fig. 2. It is shown that the electric field is homogeneously distributed in the cell except for the wires where the field is enhanced. The average electric field has one component along the direction of propagation (longitudinal plasma wave). The electric field enhancement at the wire is only about 25% because the wire axis is perpendicular to the external electric field. The plasma wavelength $\lambda_p$ is 4.8 cm, thrice larger than the primitive cell size $b=1.63$ cm. Therefore, the effective medium approximation is applicable to describe the homogeneous field in the lattice at least at the frequencies close to the plasma frequency. As we discuss later, this effective medium has SD.[5,6]

The plasma frequency was also calculated for a range of values of the ratio $r/a$ of rod radius $r$ to cubic cell length $a$ from 0.0012 to 0.18. As shown in Fig. 3 for $r/a<0.01$, the calculated plasma frequency agrees with the following equation:

$$\frac{\omega_p a}{2c} = \sqrt{\frac{2\pi}{\ln\frac{a}{r}}}, \tag{1}$$

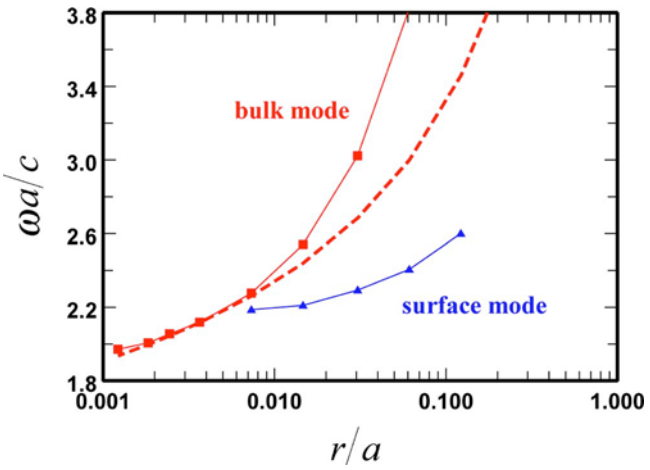


FIG. 3. (Color online) Normalized plasma frequency of bulk modes as a function of the ratio of rod radius $r$ to cubic cell length $a$ (red solid line), analytical representation of Eq. (1) (dashed line), and normalized resonance frequency of the surface mode on the anisotropic (100) interface (blue line).

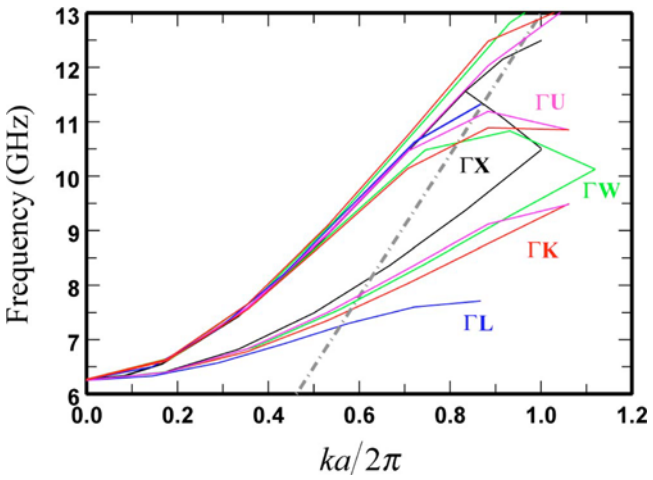


FIG. 4. (Color online) Dispersion of longitudinal (plasmon) and transverse (photon) waves. One plasmon and two photons are calculated for each of the following directions: Γ-$X$ (black), Γ-$W$ (green), Γ-$U$ (magenta), Γ-$K$ (red), and Γ-$L$ (blue). Dashed-dotted straight line is the light dispersion in vacuum.

The entire Brillouin diagram of a diamond wire lattice can be calculated by eigenmode simulations for varied phase advances between the parallel sides of the primitive cell (Fig. 2). The primitive cell is a rhombohedron with a side length of $b=a/\sqrt{2}$. The Brillouin zone of a diamond lattice[1] is characterized by the following points in the wave number **k**-space:

$$\Gamma=\frac{2\pi}{a}(0,0,0),\quad X=\frac{2\pi}{a}(1,0,0),\quad L=\frac{2\pi}{a}\left(\frac{1}{2},\frac{1}{2},\frac{1}{2}\right),$$

$$K=\frac{2\pi}{a}\left(\frac{3}{4},\frac{3}{4},0\right),\quad W=\frac{2\pi}{a}\left(1,\frac{1}{2},0\right),$$

$$U=\frac{2\pi}{a}\left(1,\frac{1}{4},\frac{1}{4}\right) \tag{2}$$

The normalized wave number $ka$ for the **k**-vector varying from the Γ-point to the points $X$, $L$, $K$, $W$, and $U$ and the corresponding phase advances $\Phi_{1,2,3}$ between the opposite sides of the primitive cell are listed in Table I. These phase advances were used in the simulation.

The results of the dispersion simulation are presented in Fig. 4 for a diamond lattice with cell length $a=2.3$ cm and wire radius $r=0.07$ cm. As the wave number $ka$ increases, the degenerate three waves at the plasma frequency in the Γ-point split into a wave longitudinal along the propagation direction (plasmon) and two transverse waves (photons).[20,21] The frequencies of the transverse modes are higher than the frequencies of the longitudinal modes. Figure 4 shows two bundles of waves (plasmon and photons) propagating in the directions listed in Table I. These bundles of waves can be identified at lower wave numbers ($ka \ll \pi$). As can be seen in Fig. 4, the longitudinal mode (plasmon) is anisotropic and the transverse modes (photons) are almost isotropic at lower wave numbers. The plasmon propagating in the direction Γ-$L$ has the lowest frequency, while the Γ-$X$ plasmon has the highest frequency.

## III. SPATIAL DISPERSION

We represent the diamond wire lattice as a medium with SD. The medium dielectric constant is a tensor with the following components:[20]

$$\varepsilon_{xx}=\varepsilon_p+\alpha_1\frac{k_x^2c^2}{\omega^2}+\alpha_2\frac{k_y^2c^2}{\omega^2}+\alpha_2\frac{k_z^2c^2}{\omega^2},$$

$$\varepsilon_{yy}=\varepsilon_p+\alpha_2\frac{k_x^2c^2}{\omega^2}+\alpha_1\frac{k_y^2c^2}{\omega^2}+\alpha_2\frac{k_z^2c^2}{\omega^2},$$

$$\varepsilon_{zz}=\varepsilon_p+\alpha_2\frac{k_x^2c^2}{\omega^2}+\alpha_2\frac{k_y^2c^2}{\omega^2}+\alpha_1\frac{k_z^2c^2}{\omega^2},$$

$$\varepsilon_{xy}=\varepsilon_{yx}=2\alpha_3\frac{k_xk_yc^2}{\omega^2},$$

$$\varepsilon_{xz}=\varepsilon_{zx}=2\alpha_3\frac{k_xk_zc^2}{\omega^2},$$

$$\varepsilon_{yz}=\varepsilon_{zy}=2\alpha_3\frac{k_yk_zc^2}{\omega^2}. \tag{3}$$

At the Γ-point, the dielectric constant is equal to the dielectric constant of isotropic plasma,

$$\varepsilon_p=1-\frac{\omega_p^2}{\omega^2}. \tag{4}$$

Even an isotropic medium with SD has nondiagonal components of the dielectric constant matrix. The coefficients $\alpha_{1,2,3}$ for the isotropic medium satisfy the equation $\alpha_1-\alpha_2=2\alpha_3$. This is not the case for the anisotropic lattice that we have analyzed. The coefficients $\alpha_{1,2,3}$ can be determined from the numerically calculated dispersion curves (Fig. 5). First, we consider the plasmon, a longitudinal mode in the direction Γ-$X$. The dispersion equation of this mode is derived from Maxwell's equations for a medium with a dielectric tensor Eq. (3) (Ref. 20) and gives

TABLE I. Phase advance range for Brillouin diagram simulation.

| Direction | Wave number $ka$ range | Phase advance $\Phi_1$ range | Phase advance $\Phi_2$ range | Phase advance $\Phi_3$ range |
|---|---|---|---|---|
| $\Gamma \rightarrow X$ | $(0,2\pi)$ | $(0,\pi)$ | $(0,\pi)$ | (0,0) |
| $\Gamma \rightarrow L$ | $(0,\pi\sqrt{3})$ | $(0,\pi)$ | $(0,\pi)$ | $(0,\pi)$ |
| $\Gamma \rightarrow K$ | $(0,3\pi/\sqrt{2})$ | $(0,3\pi/2)$ | $(0,3\pi/4)$ | $(0,3\pi/4)$ |
| $\Gamma \rightarrow W$ | $(0,\pi\sqrt{5})$ | $(0,3\pi/2)$ | $(0,\pi)$ | $(0,\pi/2)$ |
| $\Gamma \rightarrow U$ | $(0,3\pi/\sqrt{2})$ | $(0,5\pi/4)$ | $(0,5\pi/4)$ | $(0,\pi/2)$ |

$$\omega^2 = \omega_p^2 + \alpha_1 k^2 c^2. \tag{5}$$

Using the best fit to the curve in Fig. 5 we determine $\alpha_1 = -0.41$. The dispersion curve [Eq. (5)] is shown in Fig. 5 by a dashed black line. Then, the photon, a transverse mode in the direction $\Gamma$-$X$, is considered; it has the dispersion equation

$$\omega^2 = \omega_p^2 + (1 - \alpha_2)k^2 c^2. \tag{6}$$

From the best fit we determine $\alpha_2 = 0.13$. In Fig. 5, the dispersion of photons propagating in the $\Gamma$-$X$ direction is shown by solid black lines and compared to the dispersion presented by Eq. (6) (dashed black line). After that, we consider the plasmon mode in the $\Gamma$-$L$ direction. The dispersion equation is

$$\omega^2 = \omega_p^2 + \frac{1}{3}(\alpha_1 + 2\alpha_2 + 4\alpha_3)k^2 c^2. \tag{7}$$

From the fitting curve (dashed blue curve in Fig. 5) we determine $\alpha_3 = -0.17$. The plasmon mode in the $\Gamma$-$K$ direction has been checked against the dispersion equation

$$\omega^2 = \omega_p^2 + \frac{1}{2}(\alpha_1 + \alpha_2 + 2\alpha_3)k^2 c^2 \tag{8}$$

with good agreement. The result is plotted in Fig. 5 (red lines).

Therefore, the SD parameters $\alpha_{1,2,3}$ are determined for the diamond wire lattice with $a = 2.3$ cm and $r = 0.07$ cm. They can be used for modeling the surface modes on the interface of the medium with SD (see Sec. V).

## IV. SURFACE MODES

The diamond wire lattice can be built layer by layer in three different ways[18] and three different interfaces thus can be formed. The interface (100) depicted in Fig. 1(a) is formed perpendicular to the [100] direction. This interface is anisotropic because it is not symmetrical with respect to the directions [011] and $[01\bar{1}]$. The same cubic cell is shown in Fig. 1(b) but the interface (111) is oriented perpendicular to the direction $[1\bar{1}1]$. This interface is quasi-isotropic. The interface (011) perpendicular to the $[01\bar{1}]$ direction is shown in Fig. 1(c) by splitting the cell of Fig. 1(a) and extending it in the $x$-direction to better show the interface structure. The interface (011) is anisotropic.

In this way, three interfaces (one isotropic and two anisotropic) are formed. This makes the surface modes on a diamond lattice interface different from those on the isotropic interface of the simple cubic lattice studied in Ref. 6. According to the "artificial plasma" model,[2] the surface mode resonance frequency is $f_p/\sqrt{2}$ at large wave numbers. We show in Ref. 6 that the surface mode on the interface of a simple cubic lattice is strongly affected by SD and not described by the artificial plasma model. The frequency of the surface mode tends to $f_p$ at large wave numbers. As we show further for the diamond lattice, SD similarly affects the surface mode on the isotropic interface (111). The frequency of the surface mode resonance tends to $f_p$. The surface modes on the anisotropic interfaces (100) and (011) have resonance frequencies lower than $f_p$.

As a specific example, a stack of cells with the dimensions $b \times b \times 5b$ was used for a surface mode calculation [Fig. 6(a)]. This stack of cells models the anisotropic interface (100) built as shown in Fig. 1(a). The surface modes propagating in the $x$- and $y$-directions are different. A mode uniform in the $y$-direction and with a phase advance $\varphi_x = k_x b$ in the $x$-direction was calculated. The perfect-matching layer boundary condition was set on the bottom of the cell. The two periods of the lattice in the $z$-direction are used to model a semi-infinite lattice because of computational limitations. The surface mode in Fig. 6(a) with a frequency of 4.68 GHz was simulated for the phase advance $\varphi_x$ of 150°. The electric field has the longitudinal $E_x$ component at the side of the cell. The transverse component of the electric field $E_z$ points into the vertex of the diamond lattice. The average magnetic field has one component $H_y$ in the plane of the interface transverse to the propagation direction. The dispersion curve of the anisotropic interface (110) mode is

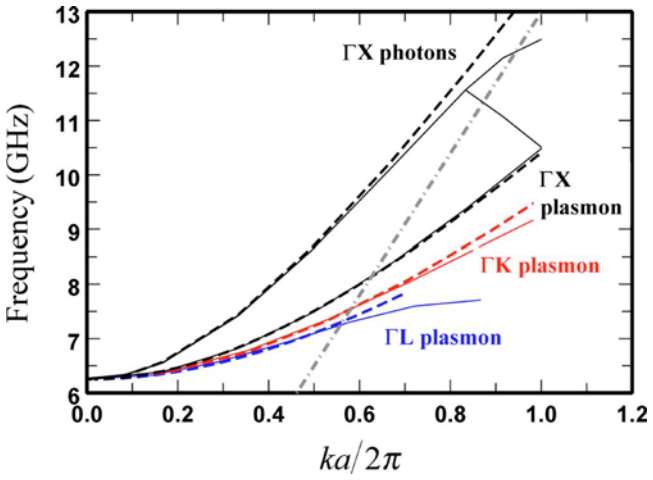


FIG. 5. (Color online) Comparison of wave dispersion in the lattice (solid lines) and the SD medium (dashed lines): $\Gamma$-$X$ plasmon and photons (black), $\Gamma$-$L$ plasmon (blue), and $\Gamma$-$K$ plasmon (red).

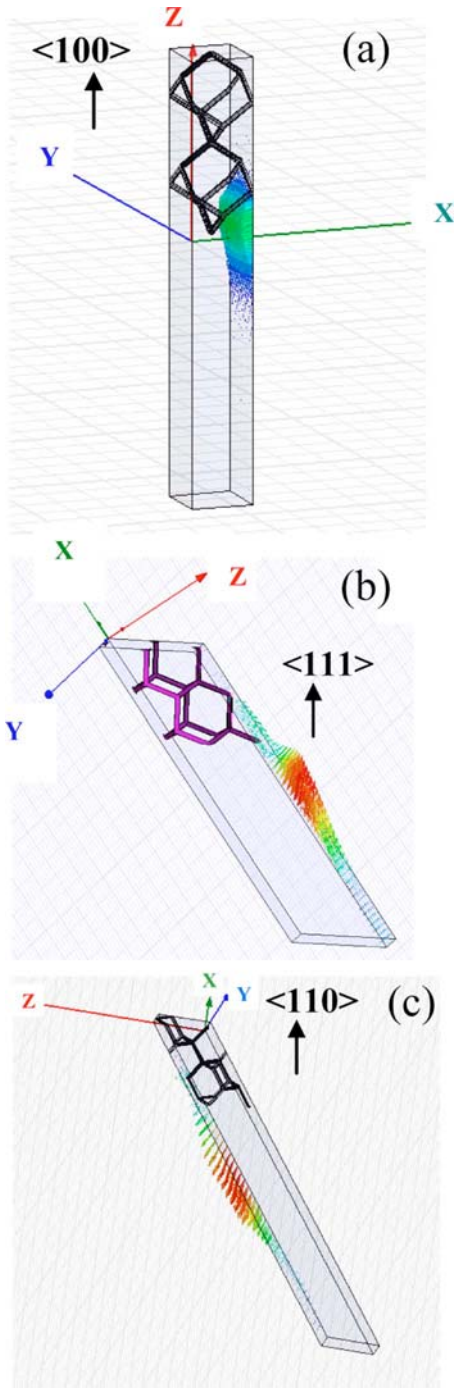


FIG. 6. (Color online) Stack of cells used for surface mode simulation on (a) the anisotropic (100) interface, (b) isotropic (111) interface, and (c) anisotropic (110) interface. The electric field distribution in the surface modes is shown.

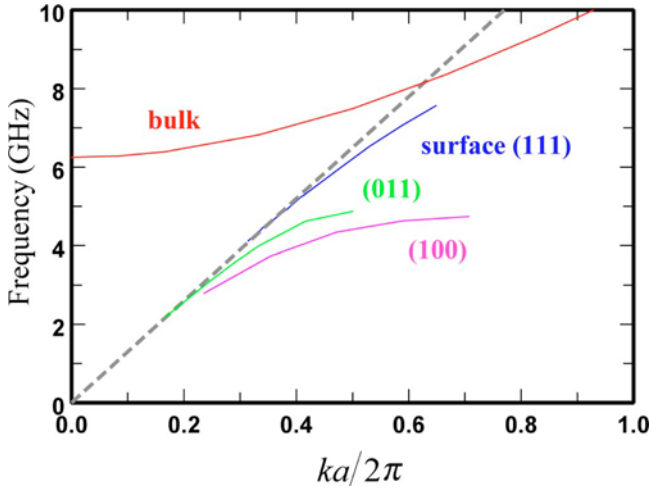


FIG. 7. (Color online) Dispersion of bulk waves and surface waves on the isotropic interface (111) and anisotropic interfaces (100) and (011) of the diamond metallic lattice. The cubic cell period is $a=2.3$ cm and wire radius $r=0.07$ cm. The dashed line depicts the light dispersion in vacuum. The frequency of the isotropic (111) interface mode tends to the plasma frequency, which disagrees with the "artificial plasma" model.

shown in Fig. 7(a). It coincides with the light cone at lower wave numbers $k_x$ and approaches the surface resonance frequency of 4.74 GHz at the maximum wave number ($k_x b = \pi$). The dispersion of the bulk plasmon mode propagating in the $\Gamma$-$X$ direction is also shown in Fig. 7 for comparison. The surface mode in the $y$-direction is different; it converts into a bulk plasmon mode with a frequency $f_p=6.25$ GHz at large wave numbers (not shown in Fig. 7).

The surface mode propagating in the $x$-direction occupies only the surface layer of the lattice [Fig. 6(a)]. The anisotropic interface with vertices on it supports this surface mode. The frequency of this mode is close to $f_p/\sqrt{2}$. However, this surface mode is not described by the artificial plasma model[2] because the interface is anisotropic. This surface mode is similar to that supported by a grating or an impedance surface. The surface modes propagating in the $x$-direction on the anisotropic interface were simulated for different metal rod radii $r$ ranging from 0.017 to 0.14 cm. The surface mode resonance frequency was found to be different from $f_p/\sqrt{2}$ in all cases. Figure 3 depicts the surface mode frequency at the maximum phase advance $k_x b=\pi$ as a function of the ratio $r/a$. The dependence on $r/a$ is slight. This is an indication that the anisotropic surface (110) acts as an impedance surface. Therefore, new properties of surface modes have been found as compared to the surface modes on the simple cubic lattice.[6]

The (111) interface is isotropic for surface waves [Fig. 1(b)]. The surface modes on this interface have been simulated and properties similar to the simple cubic lattice have been found. The cell for simulation of an isotropic (or more exactly, quasi-isotropic) interface has the form of a parallelepiped with the dimensions $b\times b\sqrt{3}\times 5b$ [Fig. 6(b)]. The number of lattice periods used for modeling was limited. Nevertheless a confined surface mode was obtained in the simulation. In Fig. 6(b), a surface mode at a frequency of 5.24 GHz for a phase advance of 180° along the longer cell side ($b\sqrt{3}$) is shown. The surface mode in the perpendicular direction, along the shorter cell side ($b$), has been simulated and yielded the same dispersion. The dispersion curve of the surface mode on the isotropic interface (111) is plotted in Fig. 7. Similar to the simple cubic lattice,[6] the surface mode curve extends to the plasma frequency, and the surface mode converts to the bulk mode. The theory of a medium with SD can be applied to the surface modes on an isotropic interface (Sec. V).

The stack of cells for simulation of the anisotropic interface (110) has the form of a parallelepiped with the dimen-

sions $b \times a$ along the interface [Fig. 6(c)]. In Fig. 6(c), the surface mode at a frequency of 3.99 GHz for a phase advance of 120° along the longer cell side (of the length $a$) is shown. The dispersion curve of the surface mode on the anisotropic interface (110) is plotted in Fig. 7. The dispersion is similar to that of the (100) interface mode.

## V. SURFACE MODE ON THE INTERFACE OF A MEDIUM WITH SPATIAL DISPERSION

The effect of SD can be qualitatively explained assuming a single nonvanishing parameter $\alpha_3$. We first formulate the boundary conditions at the isotropic interface of the lattice. The interface is in the $x$-$y$-plane, and the $z$-axis points from vacuum to the medium. We analyze the surface mode propagating in the $x$-direction. The surface mode's electromagnetic field has the components $E_x$, $E_z$, and $H_y$.

We represent the $x$-component of the electric displacement vector as

$$D_x = \varepsilon_p E_x + i\frac{k_x c^2}{\omega^2}\frac{\partial}{\partial z}(2\alpha_3 E_z), \tag{9}$$

where we have replaced the wave vector component $k_z$ with the operator $i(\partial/\partial z)$. By integrating Maxwell's equation over a contour of an infinitesimal thickness $2\delta$ drawn around the interface, we obtain

$$H_y^{(1)} - H_y^{(2)} = -i\frac{\omega}{c}\int_{-\delta}^{\delta} D_x dz, \tag{10}$$

and then wind up with the boundary condition

$$H_y^{(1)} - 2\frac{k_x c}{\omega}\alpha_3 E_z^{(1)} = H_y^{(2)}, \tag{11}$$

where indices (1) and (2) indicate "lattice" and "vacuum," respectively. The same boundary condition can be derived by matching the Poynting vector components perpendicular to the boundary. Using the $z$-component of Poynting vector in SD medium,[20]

$$S_z = \frac{c}{8\pi}\mathrm{Re}(E_x^* H_y) - \frac{\omega}{8\pi}\frac{\partial \varepsilon_{zz}}{\partial k_z}|E_z|^2 - \frac{\omega}{8\pi}\frac{\partial \varepsilon_{xz}}{\partial k_z}\mathrm{Re}(E_x^* E_z), \tag{12}$$

we can derive the boundary condition [Eq. (11)] if $\alpha_{1,2}=0$.

The electric field is continuous at the interface,

$$E_x^{(1)} = E_x^{(2)}. \tag{13}$$

Using Maxwell's equations and the boundary conditions in Eqs. (11) and (13), we derive the surface mode dispersion equation,

$$\varepsilon_p^2\left(k_x^2 - \frac{\omega^2}{c^2}\right)\left(1 + 4(\alpha_3 + \alpha_3^2)\frac{k_x^2 c^2}{\omega^2 \varepsilon_p}\right) = k_x^2 - \frac{\omega^2}{c^2}\varepsilon_p. \tag{14}$$

In an isotropic plasma ($\alpha_3=0$) the electrostatic resonance ($k_x \gg \omega/c$) of the surface waves occurs at $\varepsilon_p=-1$. Both field components $E_x$ and $E_z$ are equal and decay as $\exp(-k_x|z|)$ into the plasma and vacuum. The surface plasma resonance is sustained by the symmetrical field distributions in both vacuum and plasma. The field is localized at the surface as the dielectric constant $\varepsilon_p$ approaches the value $-1$. The balance between the fields in vacuum and in plasma falls apart as SD is introduced.

In a medium with SD (finite $\alpha_3$), the electrostatic resonance ($k_x \gg \omega/c$) occurs at $\varepsilon_p=0$ according to Eq. (14). The field in the medium is evanescent as $E_{x,z} \sim \exp(-\kappa z)$, where the decay constant $\kappa$ into the medium is expressed as

$$\kappa^2 = \frac{k_x^2 - \frac{\omega^2}{c^2}\varepsilon_p}{1 + 4(\alpha_3 + \alpha_3^2)\frac{k_x^2 c^2}{\omega^2 \varepsilon_p}}. \tag{15}$$

SD causes unbalancing of the surface mode field distributions in the medium and vacuum. In the medium with slight SD $|\alpha_3| \ll 1$, the decay constant $\kappa$ of Eq. (15) reaches its maximum at $\varepsilon_p=-1$ and decreases to zero at $\varepsilon_p=0$. For the lattice we simulated ($\alpha_3=-0.17$) the decay constant $\kappa$ stays constant at lower frequencies and decreases monotonically to zero as the frequency approaches the plasma frequency. This indicates that the surface mode in the medium is not localized at the interface and is converted into a plasmon. The surface mode in vacuum in turn becomes more localized at the interface as the frequency approaches the electrostatic resonance.

In this section, we derived the surface wave dispersion assuming $\alpha_{1,2}=0$. However, for the diamond lattice $\alpha_{1,2}$ are not equal to 0 and are determined in Sec. III by fitting the SD theory to the numerical results. We used only one nonvanishing SD parameter $\alpha_3$ to simplify the analysis. The goal was to explain why the surface wave dispersion is different from that of an isotropic plasma surface wave. A solution for all SD nonvanishing parameters $\alpha_{1,2,3}$ would be complicated. It will require auxiliary boundary conditions[20,22] to match the field in vacuum to the field formed by the superposition of the two modes in the medium with SD. We restrict ourselves to numerical simulation of the surface mode (Sec. III).

## VI. PLASMONIC WAVEGUIDE

A defect in a diamond lattice can be formed as follows. We take the lattice with the anisotropic (100) interface [Fig. 1(a)] and reflect it over the interface. The two interfaces together form the defect. The defect forms a plasmonic waveguide as shown in Fig. 8. Note that the defect cannot be formed using a simple cubic lattice. This plasmonic waveguide can be employed as an accelerator structure. Both irises and accelerator cells are formed in the defect. The iris has a cross section smaller than the surrounding lattice cells, and the actual accelerating cell (cavity) has a transverse dimension larger than the lattice cells. The iris is a rhomb with a side equal to 0.2λ, which is smaller than the iris diameter in typical disk-loaded accelerator structures. The plasmonic waveguide is analogous to a coupled-cavity structure. The defect mode can propagate at the frequencies in the band gap, below the plasma frequency. It is a TM mode with the electric field on the $x$-axis. The HOMs at frequencies higher than the plasma frequency are not confined in the defect and leak out through the lattice.

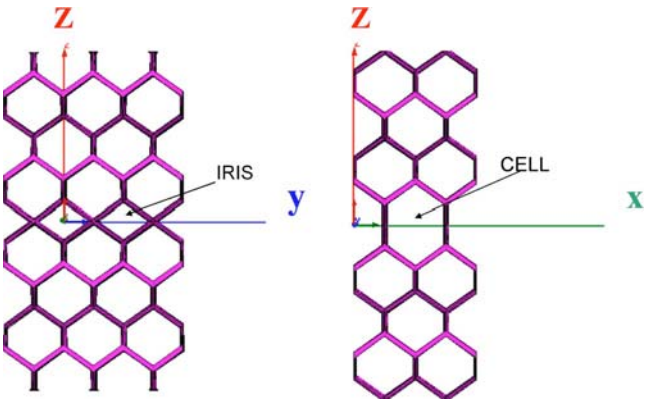


FIG. 8. (Color online) Accelerator structure using a defect in 3D metallic diamond wire lattice. An electron beam traverses in the *x*-direction.

The accelerator structure can be built if the two lattice interfaces are brought together forming a beam channel. However, in such a structure a deflecting HEM mode with low cutoff frequency exists. To avoid this effect we propose to utilize a defect in the lattice to form the structure.

HFSS simulation of the plasmonic waveguide was carried out using one stack of cells with a length of one period *b* (Fig. 9). Similar to the surface mode simulation, the phase advance conditions are set between the parallel sides in the direction of propagation *x*. The TM mode is confined as shown in Fig. 9. This mode is calculated to have a frequency of 6.02 GHz and phase advance of 150°. The dispersion of the defect and bulk modes is plotted in Fig. 10. The TM mode has a cutoff at 5.77 GHz, below the plasma frequency of 6.25 GHz. The frequency of the mode varies up to 6.03 GHz as the phase advance varies up to 180° (Fig. 10). The operating mode is close to a $\pi$-mode, and the group velocity is almost zero. This indicates that it is a coupled-cavity structure. The bulk mode in contrast has a higher group velocity than the defect mode. The deflecting HOMs fall into the propagation band of bulk modes, occupy the entire structure, and leak out with higher group velocity.

## VII. DISCUSSION

An experimental test of the diamond lattice as an accelerator structure would be very valuable. For example, at MIT, the accelerator test facility includes the Haimson Research Corp. (HRC) linear accelerator[23] and relativistic klystron[24] operating at a frequency of 17.14 GHz. The accelerator produces trains of bunches with a 17.14 GHz repetition frequency. The radiation from the train of bunches is constrained to harmonics of the accelerator bunch train frequency of 17.14 GHz.[13] For testing the diamond lattice with the electron beam in the MIT/HRC test accelerator facility, the lattice design has to be scaled to a plasma frequency of about 17.14 GHz, yielding a wire length $l=0.36$ cm and a wire radius $r=0.025$ cm. An interesting experiment would be to excite a surface mode on the lattice at 17.14 GHz using the electron bunch. The harmonics of the 17.14 GHz frequency radiate into free space and also into the lattice and can be detected. The plasmonic-waveguide-based accelerator structure is also of interest. Because of the planar geometry, side coupling into the plasmonic waveguide can be provided (along the *y*-axis in Fig. 8). These examples are for a frequency of 17.14 GHz, but a lower frequency version of this structure is also attractive. Another possibility is to build a diamond nanostructure and utilize it for laser acceleration.

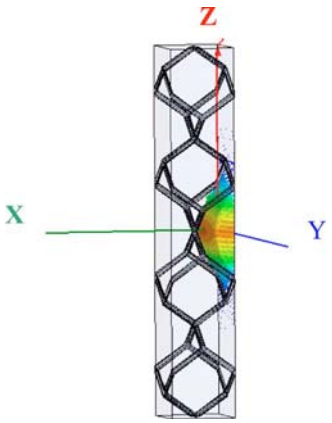


FIG. 9. (Color online) Simulation of plasmonic waveguide. The defect mode is a longitudinal TM mode propagating in the *x*-direction. The electric field distribution is shown.

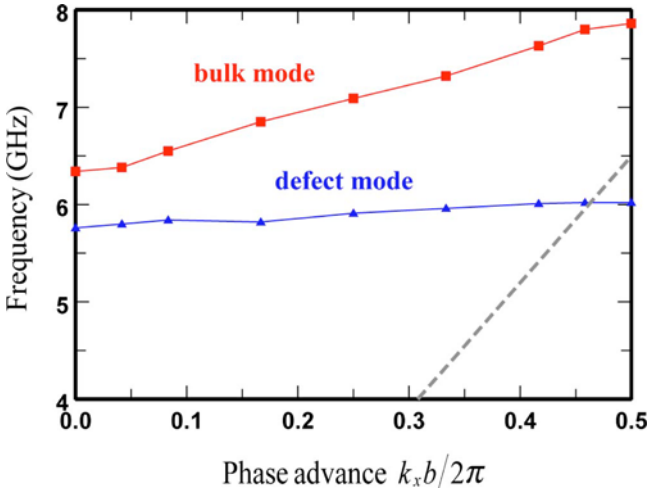


FIG. 10. (Color online) Dispersion of plasmonic waveguide modes. The defect mode is an accelerating mode. Dashed line is the light dispersion in vacuum. The cubic cell length $a=2.3$ cm and wire radius $r=0.07$ cm.

The parameters of an effective medium with SD have been determined ($\alpha_1=-0.41$, $\alpha_2=0.13$, and $\alpha_3=-0.17$) for the lattice with $r/a=0.03$. The Smith–Purcell radiation and transition radiation of a charged particle (electron bunch) passing above the interface of the effective medium can be calculated.[8] An approximation of the quasi-isotropic medium can be used to simplify the analysis. This might be a subject for future studies.

## VIII. CONCLUSIONS

3D metallic lattices are attractive for applications as high gradient accelerator structures. Being frequency selective they suppress and allow easy extraction of higher order mode wakefields generated by the electron beam in a linear accelerator. The bulk and surface modes have been calculated for the diamond wire lattice. The surface mode can be used for acceleration or beam diagnostics. Depending on the lattice interface (anisotropic or isotropic) the dispersion of the sur-

face mode is different. It is found that the surface mode is affected by the SD of the lattice. A defect in a diamond lattice can form a plasmonic waveguide with both irises and cavities. The plasmonic waveguide is proposed as a possible accelerator structure. The possibility of testing diamond wire lattices in the MIT/HRC accelerator facility was discussed.

## ACKNOWLEDGMENTS

We thank R. Marsh of MIT and E. Smirnova of LANL for helpful discussions. This work was supported by the Office of High Energy Physics, U.S. Department of Energy.

[1]D. F. Sievenpiper, M. E. Sickmiller, and E. Yablonovitch, Phys. Rev. Lett. **76**, 2480 (1996).
[2]J. B. Pendry, A. J. Holden, W. J. Stewart, and I. Youngs, Phys. Rev. Lett. **76**, 4773 (1996).
[3]W. Rotman, IRE Trans. Antennas Propag. **10**, 82 (1962).
[4]G. Shvets, AIP Conf. Proc. **647**, 371 (2002).
[5]P. A. Belov, R. Marques, S. I. Maslovski, I. S. Nefedov, M. Silveirinha, C. R. Simovsky, and S. A. Tretyakov, Phys. Rev. B **67**, 113103 (2003).
[6]M. A. Shapiro, G. Shvets, J. R. Sirigiri, and R. J. Temkin, Opt. Lett. **31**, 2051 (2006).
[7]M. G. Silveirinha and C. A. Fernandes, IEEE Trans. Microwave Theory Tech. **53**, 1418 (2005).
[8]V. L. Ginzburg and V. N. Tsytovich, *Transition Radiation and Transition Scattering* (Hilger, New York, 1990).
[9]E. I. Smirnova, A. S. Kesar, I. Mastovsky, M. A. Shapiro, and R. J. Temkin, Phys. Rev. Lett. **95**, 074801 (2005).
[10]E. I. Smirnova, I. Mastovsky, M. A. Shapiro, R. J. Temkin, L. M. Earley, and R. L. Edwards, Phys. Rev. ST Accel. Beams **8**, 091302 (2005).
[11]*Linear Accelerators*, edited by P. Lapostolle and A. Septier (North-Holland, Amsterdam, 1970).
[12]P. B. Wilson, IEEE Trans. Nucl. Sci. **26**, 3255 (1979).
[13]S. E. Korbly, A. S. Kesar, J. R. Sirigiri, and R. J. Temkin, Phys. Rev. Lett. **94**, 054803 (2005).
[14]S. E. Korbly, A. S. Kesar, R. J. Temkin, and J. H. Brownell, Phys. Rev. ST Accel. Beams **9**, 022802 (2006).
[15]R. A. Marsh, A. S. Kesar, and R. J. Temkin, Phys. Rev. ST Accel. Beams **10**, 082801 (2007).
[16]X. E. Lin, Phys. Rev. ST Accel. Beams **4**, 051301 (2001).
[17]B. Cowan, AIP Conf. Proc. **877**, 844 (2006).
[18]M. Maldovan and E. L. Thomas, Nature Mater. **3**, 593 (2004).
[19]High Frequency Structure Simulator (HFSS) Version 10, Ansoft Corp., Pittsburg, PA, 2005.
[20]V. M. Agranovich and V. L. Ginzburg, *Spatial Dispersion in Crystal Optics and the Theory of Excitons* (Wiley, New York, 1966).
[21]G. Shvets, A. K. Sarychev, and V. M. Shalaev, Proc. SPIE **5218**, 156 (2003).
[22]A. A. Maradudin and D. L. Mills, Phys. Rev. B **7**, 2787 (1973).
[23]J. Haimson and B. Mecklenburg, *1995 Particle Accelerator Conf* (IEEE, Piscataway, NJ, 1996), p. 755.
[24]J. Haimson and B. Mecklenburg, AIP Conf. Proc. **691**, 34 (2003).